Dynamics of Tungsten Erosion under ELM-Like Intense Heat Loads

L.N. Vyacheslavov[1,2], A.S. Arakcheev[1,2,3], A.V. Burdakov[1,3], I.V. Kandaurov[1],
A.A. Kasatov[1,2], V.V. Kurkuchekov[1,2], V.A. Popov[1,2], A.A. Shoshin[1,2], D.I. Skovorodin[1,2],
Yu.A. Trunev[1,2] A.A. Vasilyev[1,2]

[1]Budker Institute of Nuclear Physic SB RAS, Novosibirsk, Russia

[2]Novosibirsk State University, Novosibirsk, Russia

[3]Novosibirsk State Technical University, Novosibirsk, Russia

E-mail contact of main author: vyachesl@inp.nsk.su; vyachesl@gmail.com

Abstract. A test facility developed at the Budker Institute is designed for experimental simulation of effects of ITER-scale transient heat loads on plasma facing materials. Employing a long-pulse electron beam for creation of transients has advantages of low direct pressures on surface of material and lesser limitation of power density by vapor shielding. In addition, relative modest attendant background light allows using a set of diagnostics for observation of erosion dynamics. The set includes fast imaging in the near infrared, scattering of light of continuous wave laser on target surface and on droplets ejected from the melt layer. Formation of the crack network on the surface and its development with successive pulses was observed. Two-dimensional temperature distribution was obtained after heating at the cooling stage. Melting and detachment of sample parts were shown on severe damaged target. Propagation of the cracks along the surface was revealed with transverse microsections. Circular motion of the melted layer was found with subsequent exposures. Dynamics of tungsten particles in the ablation plume is investigated by small-angle light scattering technique and using fast CCD and ICCD cameras.

1. Introduction

Transient heat loads due to ELM type I or major disruptions are considered the main factor responsible for damage of tungsten surface in the ITER divertor. Different techniques are preparing for mitigation of heat load however some number of unmitigated transient events cannot be excluded. In these cases the heat loads can reach energy density Q_h=5-80 MJ·m^{-2}, power density q_h=5-25 GW·m^{-2} over the heating time τ_h=0.3-3 ms for type I ELMs and major disruption. These heat loads correspond to maximal heat flux parameter values F_{HF}=600-2000 MJ·m^{-2}·s$^{-0.5}$ [1, 2]. Such extremal impacts go well beyond the conditions in the modern tokamaks. For this reason special test facilities are built to test material under intense transient heat loads. The most advanced of them are the quasi stationary plasma accelerators (QSPAs). However, the plasma stream produced by QSPAs is not ideal substitution to plasma in the ITER divertor. It creates too high plasma pressure on tungsten surface and on melted layer moreover the power density absorbed by the tungsten is limited by vapor shield effect [3] by the value q_h=4.4-4.6 GW·m^{-2}. It corresponds to heat flux parameter F_{HF}=70-100 MJ·m^{-2}·s$^{-0.5}$ [4]. Long pulse electron beam (LPEB) produces negligible direct pressure and has much higher limit of absorbed power density due to vapor shied effect [5]. Besides, LPEB creates relatively low background light which facilitates operation of diagnostics. All the above makes LPEB attractive for simulation of transient heat load under conditions different from those in QSPAs. The following text presents a description of the test facility based on LPEB, which is developed at the Budker Institute, and some of the obtained experimental results.

2.   Test Facility

2.1. Electron Beam Source

The test facility is based on a high-power sub-millisecond electron beam injector with a plasma emitter. Total power of the device is up to 7 MW with a typical pulse duration of 0.1-0.3 ms. Target is placed in magnetic field of ~0.2 T, which is used to compress the electron beam and for generation of intense energy load on an area of 1-2 cm^2. Temporal shape of the heating has rectangular profile with sharp edges. The cross-sectional distribution of the energy load has a dome-like form with a full width at half maximum of 9-12 mm depending on magnetic field. The machine is able to provide 25 GW·m^{-2} heating power density absorbed in a tungsten target in maximum at high-power operating mode and F_{HF} >300 MJ·m^{-2}·s$^{-0.5}$. The details of the facility operation with the tungsten target are described elsewhere [6].

2.2. Diagnostics Layout

The facility is equipped with two sets by four diagnostic ports as it can be seen from Fig. 1. Set 1 is located in the target plane and is designed for observation of the ablation plume from the side closer to the target. Here spectroscopy with spatial resolution is employed as well as dust measurements system, which consisted of small angle light scattering and fast CCD and ICCD cameras. Typically we use 1.4 megapixel CCD cameras with minimal exposure time of 7 µs and 0.8 megapixel ICCD with minimal exposure 1 µs. Set 2 is located at 41 cm from the target closer to the electron beam injector and is employed for frontal observation of the target.
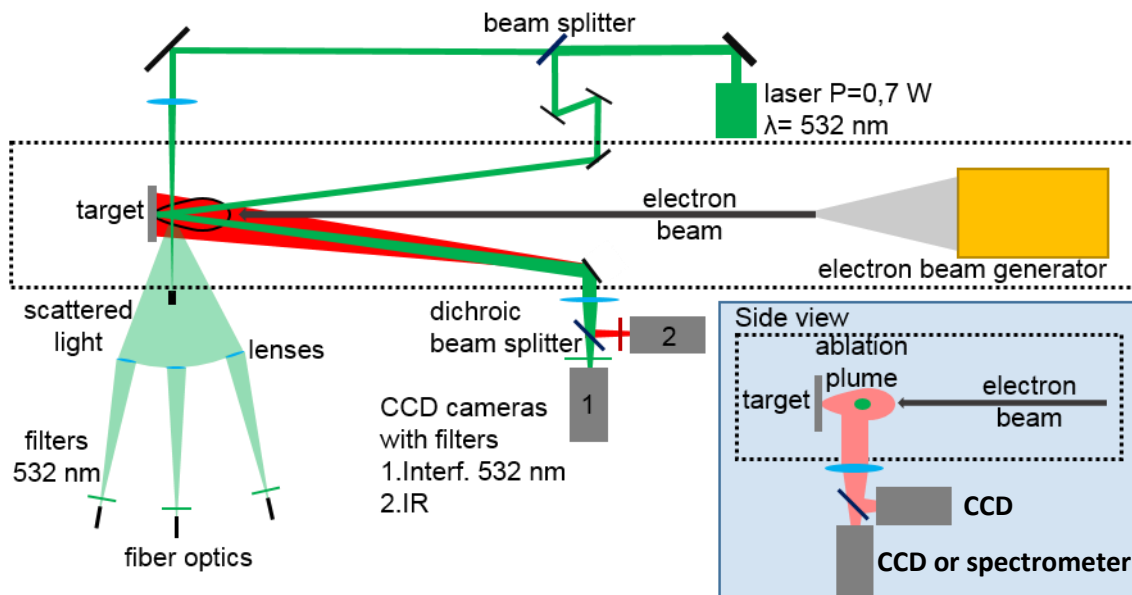

FIG. 1. Schematics of the optical diagnostics. Surface erosion is observed using CCD camera in the near infrared (NIR) range and CCD camera with green laser light illumination and narrowband interferential filter. Also 3-channel laser scattering system and position of spectrometer are shown.

Front view of the tungsten plate is captured by a fast CCD camera with 1.4 MP resolution supplied with an infrared filter. The final spectral sensitivity of the system enables to obtain a picture of thermal radiation in near infrared range (880 − 1020 nm) without interference from the light of ablation plume. Optical magnification is 1/2.7. It determines spatial resolution of the images, which is about 20 µm. 2D distribution of the surface temperature is reconstructed using absolute calibration with tungsten ribbon lamp. Also, sample surface is imaged by a

similar CCD camera applying the same optical layout using the light of a continuous wave laser (λ=532 nm). Rejection of plasma light and thermal radiation is provided by a narrowband optical filter. Laser spot is about 8 mm in diameter and cover half of the exposure area. Formation of the melted layer on crack edges and crack intersections can be detected by this diagnostics set. Surface image is transferred on an array of fiber optics equipped with IR-filter. Thermal radiation from 4 points of the surface (~2.7 mm in diameter) is gathered and recorded with photodiodes and high-frequency ADC [7]. This diagnostics can be used to investigate temperature dynamics of the surface during heat load.

The technique of small-angle scattering of continuous-wave laser light and fast visualization of droplets are used to observe the dynamics of dust particles emitted from the target during and after the pulsed heating. The laser has the following characteristics: λ = 532 nm, output power P = 0.7 W. The probe laser beam is parallel to the target surface at distance of 5-7 mm from it. The light scattered by dust particles is collected by lenses into inputs of 1 mm-diameter silica fibers and directed to the three recording channels based on PMT. The scattered light is recorded in three different angular ranges relative to the incident laser beam (0.01-0.03 rad, 0.07-0.09 rad, 0.1-0.12 rad). Fast CCD and ICCD cameras are used for observation of dust particles. Imaging of hot particles without laser illumination with 2-500 μs exposure enables measurement of particle velocities after heating pulse.

3. Experimental Results and Discussion

3.1. Crack Formation and Propagation on Tungsten Sample

Samples of rolled tungsten with thickness of 3-4 mm were used in following experiments on high heat loads. IR-imaging revealed formation non-uniformity in thermal radiation of the surface. Average energy load of 0.8 MJ·m^{-2} near melting threshold caused cracking of the tungsten sample. Crack edges were clearly detected during electron beam impact because of their increased thermal radiation (Fig. 2). It was found that slight crack net forms after first heat load. It becomes denser and more distinguishable during subsequent heat exposures. Propagation of this structure becomes slower after fourth pulse.
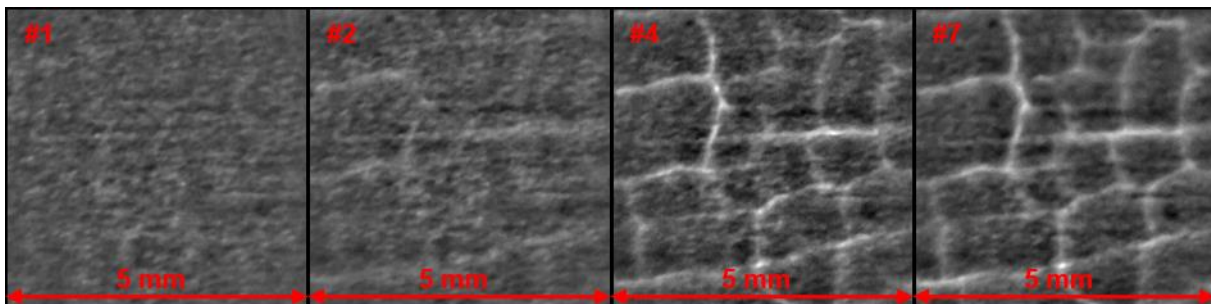

FIG. 2. Images of the central area of the target soon after heat load (1st, 2nd, 4th and 7th). Dome-like background light profile was subtracted for emphasizing of thermal radiation inhomogeneities.

Further exposures lead to increase of the sample erosion. The initially damaged tungsten target with crack network was imaged after beam impact with average energy load ~1 MJ/m^2 and F_{HF}~ 70 MJ·m^{-2}·s$^{-0.5}$. 2D temperature distribution was obtained from IR-image 20 μs after the heat load end (Fig. 3a). It shows material melting near the crack edges in the center of the target. Evidences of material melting at same places are also obtained from the target imaging in the light of continuous laser [8]. Subsequent SEM survey showed intense melting of the surface layer near these areas (Fig. 3b). Following transverse microsection of the target revealed propagation of the cracks along the surface at a depth 0.1-0.2 mm (Fig. 3c). Such cracks start from perpendicular ruptures and develop into the material bulk. This target

damage can leads to creation of detached parts of the sample. All these damages are responsible for suppression of the heat transport from the surface and can lead to appearance of the areas with excessive temperature and
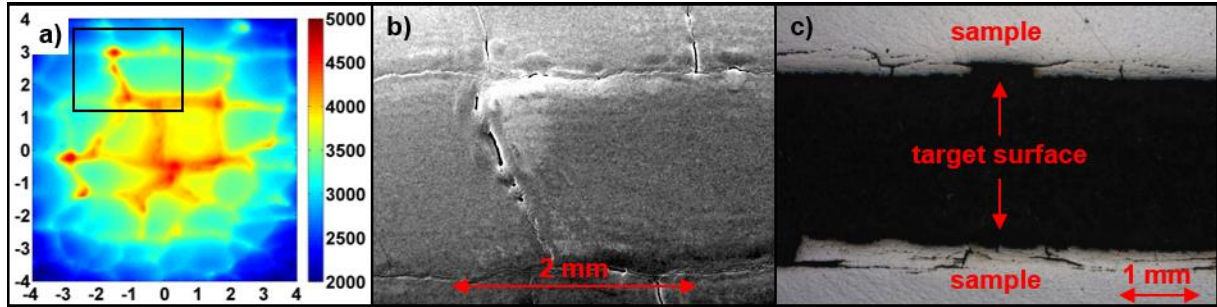

FIG. 3. a) picture of temperature distribution on the surface 20 μs after beam impact; b) SEM image of the area marked with black rectangular on (a); c) transverse microsection of the sample

3.2. Appearance of Detached Parts and Overheated Areas

Investigation of the target surface after impact of more than 100 exposures with heat loads of ~1 MJ·m^{-2} and F_{HF}~90 MJ·m^{-2}·s$^{-0.5}$ showed existence of the local hot areas (Fig. 4). These overheated regions remained on the sample during more than 5 ms after beam termination. Temperature excess over surrounding space was about 500K. Following SEM survey detected severe detachment of the tungsten layers from the bulk of the material (Fig. 4d).
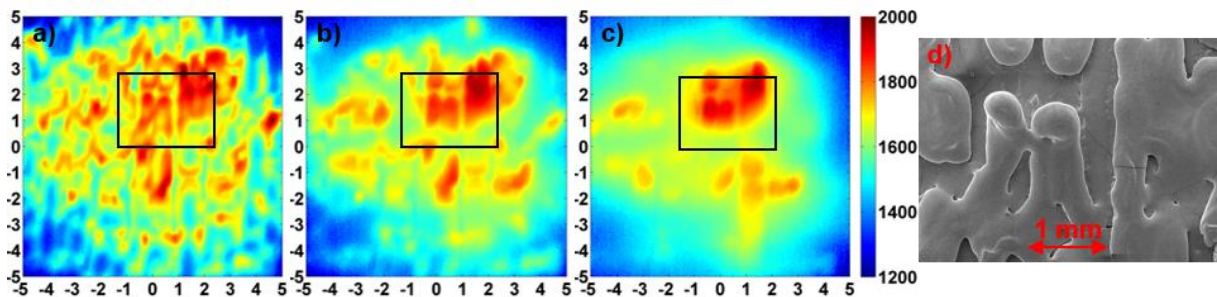

FIG. 4. Temperature distribution after electron beam termination in different times: a) 350μs, b) 1850 μs, c) 7850 μs. d) SEM picture of the area marked with black rectangular on previous images.

3.3. Imaging of Melt Tungsten

Application of CCD cameras to fast imaging of melted layer during the heating pulse is shown in Fig. 5. Spatial non-uniformities of size ≤ 1 mm are faintly visible in the thermal image but become clearer (b) after subtraction of smoothed bell-like thermal emission profile from the initial image (a). The preliminary temperature profile recovered from the thermal image with the use of absolute calibration with the tungsten ribbon lamp shows the wide area at temperature above the melting point. The temperature of central part of the melted area with diameter of 5-6 mm approaches the boiling point at the atmospheric pressure. Typically, an intense emission of droplet occurs at high heat loads basically from this central region [9]. To relate melt layer motion and droplet ejection the CCD imaging system was upgraded. The upgrade includes operation of 4 independent CCD cameras, which are seeing the same area on the tungsten target. The cameras are triggered independently with adjustable delay. Fig. 5 shows 4 frames with exposition time of 10 μs and relative delay from each other of 20 μs. The heating pulse length is 0.2 ms and exposure time for CCD start at 0.12, 0.14, 0.16 and 0.18 ms that means that all images are obtained during the heating pulse. The images are high pass filtered similarly to Fig. 5b. The frame spatial dimension is 14x14 mm. Here again the

pattern with characteristic sizes near 1mm is clearly seen. Considerable variation of the pattern between frames separated by 10 µs signifies that melt movement occurs rather fast.

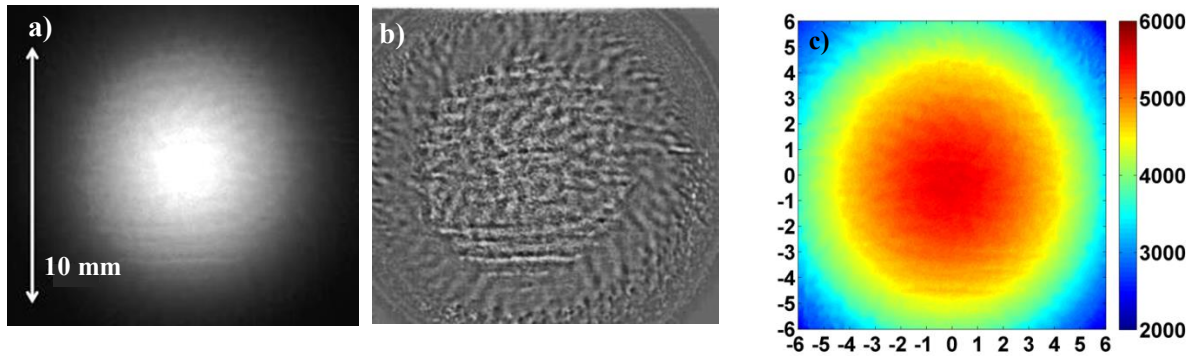*FIG. 5.   Thermal image of the tungsten target obtained during   the heating pulse   within last 10µs before the pulse end (a), and the same image as (a) but filtered by the high-pass spatial filter (b); temperature profile, obtained from thermal image using the absolute calibration (c).*
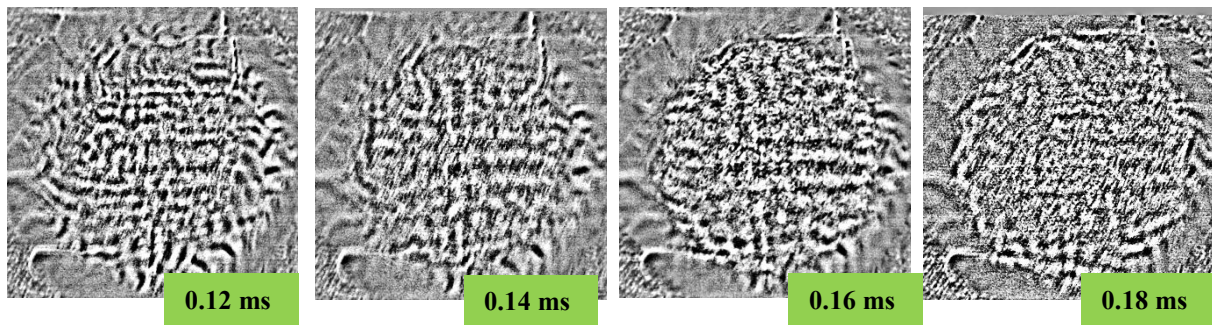

FIG. 6. NIR images of tungsten melt layer obtained during a single heating pulse of length 0.2 ms and filtered with digital spatial high-pass filter. Start time of each frame with exposure of 10 µs is shown under each image. The each image covers the area 14x14 mm on the target.

3.4.Motion of Melted Layer

Fig. 6 shows 4 frames with exposition time of 10 µs and relative delay from each other of 20 µs. The heating pulse length is 0.2 ms and exposure time for CCD start at 0.12, 0.14, 0.16 and 0.18 ms that means that all images are obtained during the heating pulse. The images are high pass filtered similarly to Fig. 5b. The frame spatial dimension is 14x14 mm.   Here again the pattern with characteristic sizes near 1mm is clearly seen. Considerable variation of the pattern between frames separated by 10 µs signifies that melt movement occurs rather fast.Multiple exposures with average heat load certainly above the melting threshold (F_{HF}>100 MJm^{-2}s$^{-0.5}$) caused formation of helical structure in thermal radiation pictures of the target surface near the border of irradiation area. Comparison of the successive NIR images 100 µs after beam ending revealed a circular motion of this structure (Fig. 7(a,b)). Electron current flows from edge to centre of the target and magnetic field is directed perpendicularly from the surface, so direction of this motion correlates with J×B force. Series of five subsequent pictures showed that helical structure on a radius of 5 mm moved on a distance of ~0.1 mm per heating pulse.
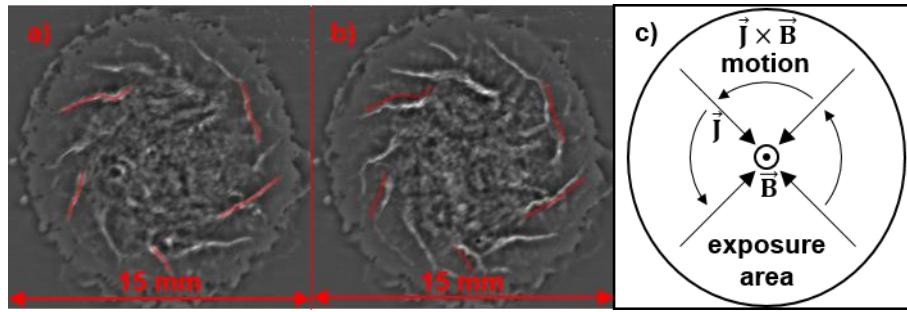
FIG. 7. Picture of melted layer motion. a) reference IR image obtained after heat load ending; b) IR image captured after 4 successive exposures; c) directions of the magnetic field, current and J×B motion. Red curves on (b) mark inhomogeneities on (a)

3.5. Laser scattering on dust particles

The waveforms of the scattering signal are shown in Fig. 8. The curves corresponding to signals in different channels are labeled in the Fig. 8 by characteristic sizes of particles. The duration of scattering signal is variable and is typically a few milliseconds. Waveform analysis shows that relatively small particles (1-4 μm) reach the laser beam before the larger particles (6+ μm), and consequently small particles have greater velocity (100+ m·s^{-1}) than the larger one.
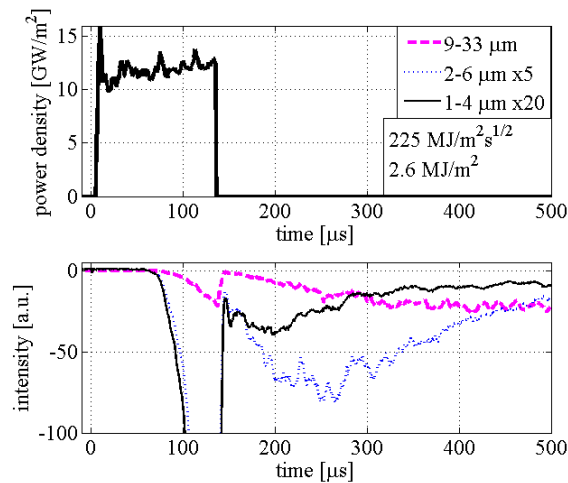

FIG. 8. Waveforms of heat load (top) and scattering signals (bottom) (magenta - 0.02 rad; blue - 0.08 rad; black - 0.11 rad).

3.6. Imaging of dust particles

Fast imaging with CCD and ICCD cameras detect particles with velocities of several hundred m/s for particles near the front of the ablation plume (Fig. 9a). At larger delays of 0.5 ms (Fig. 9b) and 1.5 ms velocities are lower 5-20 m·s^{-1} and 1-15 m·s^{-1} respectively under the heat load 2.1-2.6 MJ·m^{-2}. Noticeably, that these delays particle follow a sort of "Hubble's law" when particle velocity is proportional to the particle distance from the target surface (Fig. 10a). The start time of the ejection of dust particles approximately corresponds to the end the beam (Fig. 10b). Analysis of fast imaging of tungsten particles obtained simultaneously with laser scattering show that particles are generated during the time interval, which is much shorter than characteristic duration of laser scattering signal.
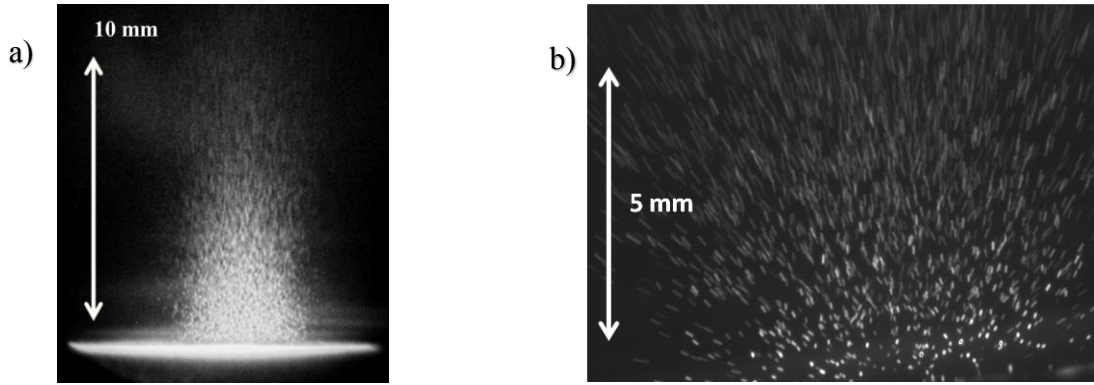
FIG. 9. Image of tungsten dust particles. a) ICCD, exposure start time, Tstart = 170 μs; exposure duration, Texp = 2 μelectron beam duration, Tbeam = 125 μs. b) CCD, Tstart = 500 μs, Texp = 20 μs, Tbeam = 131 μs.
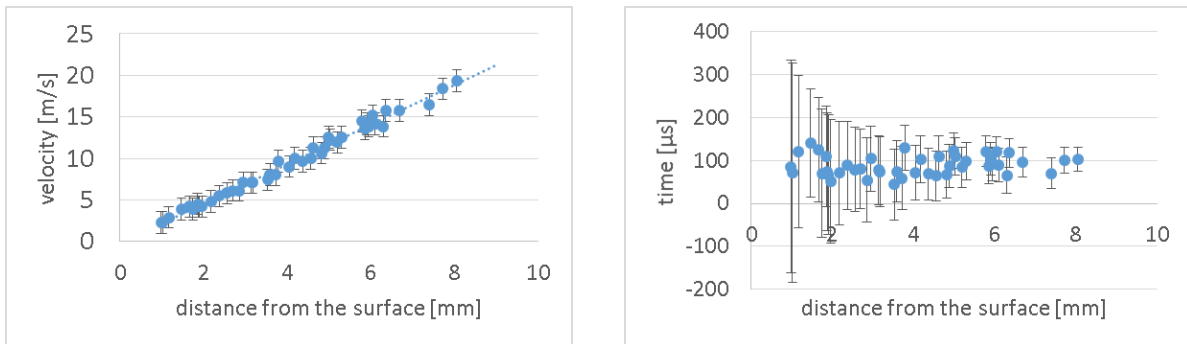

FIG. 10. Particle velocities (a) and the start time of particle ejection (b) versus distance from the surface (0 μs corresponds to the beginning of the beam injection, the electron beam duration Tbeam = 131 μs).

4. Summary

An electron beam with duration of 0.1-0.3 ms and power up to 7 MW is applied for simulation of the ITER-scale transient heat load on tungsten target. The power density, absorbed by the target, reaches 25 GW·m^{-2} in the high-power operating mode with F_{HF} >300 MJ·m^{-2}·s$^{-0.5}$ at the area of 5-7 mm in diameter. The new test facility based on this electron beam uses a set of diagnostics that are novel for this research field: small angle scattering of continuous wave (cw) laser light and fast target and droplets imaging during the heating process. The imaging of the target can be performed in two modes simultaneously: in the light of cw laser and in the near infrared range. It permits observation of dynamics of tungsten melt layer and is important for elucidation of mechanism of droplet ejection from the melt layer. Small angle light scattering is designed for investigation of dynamics of the emitted material structure as well as for estimation the amount of ejected material.

Crack network formation and development was observed with serial heat loads. Melting of the crack edges was found from 2D temperature distribution obtained from thermal images and from the target visualization using laser light illumination. Propagation of the crack along the surface was revealed with cross-section cutting. Detached parts of the target with excessive temperature of ~500 K over surrounding sample were found after more than 100 shots. Circular motion of the melted layer was detected through comparison of IR-images after heat load ending with serial of successive pulses. Preliminary results show temporal variation of small-scale structure of melt layer are presented.

Fast imaging with ICCD camera permits detection of particles with velocities of several hundred m/s near the front of the ablation plume. At larger delays of 0.5 and 1.5 ms velocities are lower 5-20 m·s^{-1} and 1-15 m·s^{-1} respectively at heat load 2.1-2.6 MJ·m^{-2}. It is significant, that at these delays particle suite sort of "Hubble's law" when the particle velocity is proportional to the particle distance from the target surface. The generation of dust particles starts with 170±15 MJ·m^{-2}·s$^{-0.5}$ and grows rapidly with an increase in the heat load. The dust particles with a size of 2-7 μm are observed.

5.   Acknowledgments

References

[1]   PITTS, R.A., et al., "A full tungsten divertor for ITER: Physics issues and design status", J. Nucl. Mater. **438** (2013) S48.

[2]   SHIMADA, M., et al., "In-vessel dust and tritium control strategy in ITER", J. Nucl. Mater. **438** (2013) S996.

[3]   SKOVORODIN, D.I., et al., "Vapor shielding models and the energy absorbed by divertor targets during transient events", Phys. Plasmas **23** (2016) 022501.

[4]   GARKUSHA, I.E., et al., "Experimental study of plasma energy transfer and material erosion under ELM-like heat loads", J. Nucl. Mater. **390-391** (2009) 814.

[5]   POPOV, V., et al., "Theoretical Modeling of Shielding for Plasma Flow and Electron Beam Heating", AIP Conf. Proc. (Proc. 11th International Conference on Open Magnetic Systems for Plasma Confinement, 2016), in press.

[6]   TRUNEV, Yu.A., et al., "Heating of tungsten target by intense pulse electron beam", AIP Conf. Proc. (Proc. 11th International Conference on Open Magnetic Systems for Plasma Confinement, 2016), in press.

[7]   IVANOVA, A.A., et al., "Pulse-signal digitizer for high-temperature plasma diagnostic systems", Instrum. Exp. Tech., **59(3)** (2016) 344–350.

[8]   VASILIEV, A.A., et al., "Observation of the Tungsten Surface Damage under ITER-relevant Transient Heat Loads during and after Electron Beam Pulse", AIP Conf. Proc. (Proc. 11th International Conference on Open Magnetic Systems for Plasma Confinement, 2016), in press.

[9]   KASATOV, A.A., et al., "Observation of Dust Particles Ejected from Tungsten Surface under Impact of Intense Transient Heat Load", AIP Conf. Proc. (Proc. 11th International Conference on Open Magnetic Systems for Plasma Confinement, 2016), in press.